Inorganic Chemistry

ARTICLE

pubs.acs.org/IC

Pro-porous Coordination Polymers of the 1,4-Bis((3,5-dimethyl-1*H*-pyrazol-4-yl)-methyl)benzene Ligand with Late Transition Metals

Aurel Tăbăcaru,*[,†] Claudio Pettinari,[†] Norberto Masciocchi,[‡] Simona Galli,*[,‡] Fabio Marchetti,[§] and Mariglen Angjellari[†]

[†]Scuola di Scienze del Farmaco e dei Prodotti della Salute, Università di Camerino, Via S. Agostino 1, 62032 Camerino, Italy

[‡]Dipartimento di Scienze Chimiche e Ambientali, Università dell'Insubria, Via Valleggio 11, 22100 Como, Italy

[§]Scuola di Scienze e Tecnologie, Università di Camerino, Via S. Agostino 1, 62032 Camerino, Italy

Supporting Information

ABSTRACT:

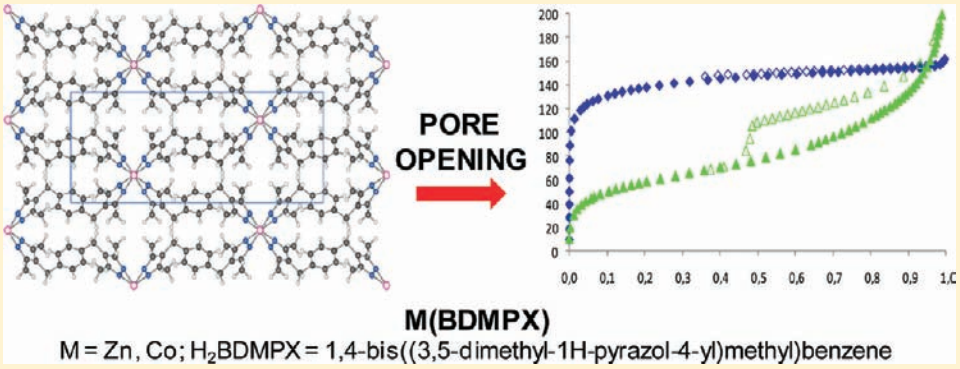

Solvothermal reactions of the flexible, pyrazole-based 1,4-bis((3,5-dimethyl-1*H*-pyrazol-4-yl)methyl)benzene ligand (H_2BDMPX) with late transition metal ions allowed the isolation of the four coordination compounds M_x(BDMPX) (x = 1 for M = Zn, **1**; Co, **2**; Cd, **3**; x = 2 for M = Cu, **4**). The investigation of the thermal behavior assessed the high thermal robustness of these materials, which are stable in air at least up to 300 °C, with the Cd(II) derivative starting to decompose only around 500 °C. As retrieved by ab initio X-ray powder diffraction, the isomorphous compounds **1**−**3** possess a dense 3-D network featuring rhombic motifs hinged about rigid and parallel chains of tetrahedral MN_4 chromophores. As demonstrated by thermodiffractometric measurements, temperature increase triggers framework flexibility. The latter is at work also when N_2 adsorption is assayed at 77 K: **1** and **2** show permanent porosity, with BET and Langmuir specific surface areas of 515, 667 m^2/g and 209, 384 m^2/g, respectively. **1** and **2** thus represent an intriguing example of "porosity without pores", their pro-porous nature being explained in terms of the flexibility of the rhombic motifs, stimulated by the gas probe and facilitated by the nature of the ligand.

1. INTRODUCTION

The vast class of porous materials, including natural clays and synthetic zeolites, possess a long-term tradition in industry due to the size- and shape-selective properties they display, imparted by their pervious pores. Though spanning a rather ample size range, the cavities and channels in naturally occurring porous materials and in synthetic zeolites do not possess the versatility nowadays attainable, through crystal engineering techniques, with porous coordination compounds (PCPs).[1] In PCPs, the sagacious coupling of metal-based nodes and O or N donor organic spacers allows one to address the network topology, the size, and the decoration of pore walls and entrance windows specific for the application under implementation. This undisputable advantage is further enhanced by the chemical (pre-[2] or postsynthetic[3]) modifications that can be carried out on the organic moieties themselves. As a matter of fact, accessible cavities and channels grant key industrial applications of economical, energetic, and environmental relevance, such as storage[4] or separation[5] of, for example, small molecules of gas or volatile organic compounds. Less investigated, yet of comparable relevance, is their usage as nanosized reactors in catalysis[6] or as nanocarriers for drug delivery and imaging.[7]

In the light of this, it is certainly not surprising that the interest in constructing PCPs with optimized supramolecular structures, leading to tailored and enhanced functionalities, has permanently increased during the last two decades. As a result, the number of porous systems prepared and characterized has been enormously augmented. Important fallout of this research, network flexibility, initially classified as an academic curiosity, when not as an

Received: July 5, 2011
Published: October 20, 2011

Scheme 1. 1,4-Bis((3,5-dimethyl-1*H*-pyrazol-4-yl)methyl)-benzene, H_2BDMPX

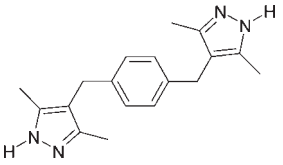

annoying aspect, has been definitely recognized as an added value,[8] allowing adsorption performances which cannot be reached by rigid PCPs. The MIL-53[8d] and M(1,4-BDP) materials (M = Ni,[9] Co;[10] 1,4-H_2BDP = 1,4-bis(1*H*-pyrazol-4-yl)benzene), existing in closed- or open-pore forms depending on the external stimulus, are among the recent notable examples in this respect.

Irrespective of their functionality, only materials possessing also a remarkable chemical and thermal inertness are likely to be useful in suitably devised applications. Our long-term experience has demonstrated that polyazolates, in which N donor heterocyclic rings are bridged by rigid or partially flexible aromatic cores, lead to the formation of materials in which key structural topologies are coupled to uncommon thermal and chemical stabilities. As a matter of fact, as shown by us and by other research groups,[2a,11] N donor spacers offer metal−ligand coordinative bonds which are stronger and less prone to hydrolysis than the O donor counterparts.[12] In this search for N donor spacers imparting robustness to the corresponding PCPs, pyrazolates have definitely surpassed the imidazolate-, triazolate-, and tetrazolate-based analogues. Examples in this direction, possessing decomposition temperatures, in air, greater than 400 °C, are Cu_2(TMBPZ), (H_2TMBPZ = 3,3′5,5′-tetramethylbispyrazole);[13] M(1,4-BDP) (M = Co;[10a] Ni, Zn[9]); Zn(1,3-BDP) (1,3-H_2BDP = 1,3-bis(1*H*-pyrazol-4-yl)benzene);[14] $Ni_8L_6(OH)_4(H_2O)_2$ (H_2L = 4,4′-bis-(1*H*-pyrazol-4-yl)biphenyl, or 2,6-bis(1*H*-pyrazol-4-yl)pyrrolo-[3,4-*f*]isoindole-1,3,5,7(2*H*, 6*H*)-tetrone);[15] $Ni_3(BTP)_2$ (H_3BTP = 1,3,5-tris(1*H*-pyrazol-4-yl)benzene), which is also capable of resisting harsh conditions such as boiling water or boiling acidic or basic aqueous environments.[16]

After having assayed rigid pyrazolates, we turned our attention to the N donor ligand 1,4-bis((3,5-dimethyl-1*H*-pyrazol-4-yl)methyl)-benzene (H_2BDMPX, Scheme 1), in which the two pyrazolyl rings are separated by a *p*-xylylene fragment.

The flexibility about the torsion angles hinged at the two methylene groups, in principle, allows H_2BDMPX to adopt *anti* (C_{2h}), *syn* (C_{2v}), or even less symmetric conformations, depending on the relative orientations of the two external arms. Thus, the carbon chain of H_2BDMPX may be a "weak point" in the framework of a coordination polymer,[17] whose flexibility, in the presence of an external stimulus, is accompanied by a change in the ligand conformation. A prototypical example in this respect is the use of 1,2-dipyridylglycol (dpyg) as a pillar in [Cu_2(pzdc)$_2$(dpyg)] (pzdc = pyrazine-3,5-dicarboxylate), which exhibits expansion/contraction phenomena during adsorption.[18]

After the first report appeared 45 years ago,[19] H_2BDMPX was subsequently adopted by Muehlebach,[20] aiming at obtaining thermosensitive organic polymers, and by Trofimenko,[21] reporting its coordination behavior toward triethylborane. Almost 40 years after, recognizing the potential of H_2BDMPX to engineer stable porous materials, we report the first examples of coordination compounds of formula M_x(BDMPX) (x = 1 for M = Zn, **1**; Co, **2**; Cd, **3**; x = 2 for M = Cu, **4**), coupling this polytopic spacer to late transition metal ions. Thermogravimetric analyses showed the high thermal robustness of these materials, which are stable in air at least up to 300 °C, with the Cd(II) derivative decomposing around 500 °C. As demonstrated by state-of-the-art powder diffraction methods, at room temperature, species **1**−**3** possess closed-pore 3-D frameworks, in which rhombic motifs can be devised. Nevertheless, external stimuli such as temperature increase or N_2 assaying at 77 K trigger framework flexibility toward an open-pore form. **1** and **2** thus represent an interesting example of "porosity without pores", their pro-porous nature being retraceable to the flexibility of the rhombic motifs, stimulated by the external probe and facilitated by the nature of the ligand.

2. EXPERIMENTAL SECTION

2.1. Materials and Methods. All of the chemicals and the reagents used were purchased from Sigma Aldrich Co. and used as received without further purification. All of the solvents were distilled prior to use. IR spectra were recorded from 4000 to 650 cm^{-1} with a Perkin-Elmer Spectrum 100 instrument by total reflectance on a CdSe crystal. Solution ^{1}H NMR spectra were measured with a VXR-300 Varian spectrometer (400 MHz) operating at room temperature and using tetramethylsilane (TMS) as the internal standard. Positive electrospray mass spectra were acquired with a series 1100 MSI detector HP spectrometer, using CH_3OH as the mobile phase. Elemental analyses (C, H, N) were performed with a Fisons Instruments 1108 CHNS-O elemental analyzer. Melting points were recorded with an SMP3 Stuart instrument mounted on a capillary apparatus. Thermal gravimetric analyses (TGA) were carried out in a N_2 stream with a Perkin-Elmer STA 6000 simultaneous thermal analyzer (heating rate: 7 °C/min). Solid-state photoluminescence spectra were collected at room temperature with a Perkin-Elmer LS 45 luminescence spectrometer equipped with a pulsed Xe flash lamp.

2.2. Synthesis of 1,4-Bis((3,5-dimethyl-1*H*-pyrazol-4-yl)-methyl)benzene. The synthesis of 1,4-bis((3,5-dimethyl-1*H*-pyrazol-4-yl)methyl)benzene (H_2BDMPX) was accomplished by improving the two-step approach already proposed in the literature[20] with an optimized procedure to purify the intermediate. Details on the synthetic procedure adopted and on the characterization of the ligand are available in the Supporting Information.

2.3. Synthesis of Zn(BDMPX) (1). H_2BDMPX (73.5 mg; 0.25 mmol) was dissolved in 15 mL of CH_3OH; then, $Zn(CH_3COO)_2$ (45.75 mg; 0.25 mmol) was added. A suspension formed which was left under stirring at 130 °C in a high-pressure glass tube for 24 h. The white precipitate obtained was filtered off, washed twice with MeOH, and then dried under vacuum. Yield: 65%. **1** is insoluble in alcohols, DMSO, acetone, CH_3CN, DMF, and water. IR (cm^{-1}): 3100−3000(vw) ν(C−$H_{aromatic}$), 3000−2800(m) ν(CH_3, CH_2), 1508(vs) ν(C═C +C═N). Elemental analysis calcd for $C_{18}H_{20}N_4Zn$ (FW = 357.8 g/mol): C, 60.43; H, 5.63; N, 15.66. Found: 60.12; H, 5.48; N, 15.37.

2.4. Synthesis of Co(BDMPX) (2). H_2BDMPX (73.5 mg; 0.25 mmol) was dissolved in 15 mL of CH_3OH; $Co(CH_3COO)_2\cdot 4H_2O$ (62.2 mg; 0.25 mmol) was then added. The violet suspension formed was left under stirring at 130 °C in a high-pressure glass tube for 24 h. The violet precipitate obtained was filtered off, washed twice with CH_3OH, and then dried under vacuum. Yield: 89%. **2** is insoluble in alcohols, DMSO, acetone, CH_3CN, DMF, and water. IR (cm^{-1}): 3100−3000(vw) ν(C−$H_{aromatic}$), 3000−2800(m) ν(CH_3, CH_2), 1507(vs) ν(C═C+C═N). Elemental analysis calcd for $C_{18}H_{20}CoN_4$ (FW = 351.3 g/mol): C, 61.54; H, 5.74; N, 15.95. Found: C, 61.12; H, 5.66; N, 15.65.

dx.doi.org/10.1021/ic2013705 |*Inorg. Chem.* 2011, 50, 11506–11513

Table 1. Crystallographic Data for the Ligand H_2BDMPX and for the Coordination Polymers 1−3

	H_2BDMPX	1	2	3
empirical formula	$C_{18}H_{22}N_4$	$C_{18}H_{20}ZnN_4$	$C_{18}H_{20}CoN_4$	$C_{18}H_{20}CdN_4$
T, °C	25	25	25	25
FW, g mol^{-1}	294.4	357.8	351.3	404.8
crystal system	monoclinic	orthorhombic	orthorhombic	orthorhombic
ρ, g/cm^3	1.22	1.46	1.43	1.57
μ(Cu Kα), cm^{-1}	5.83	22.11	82.59	102.00
F(000)	316	744	732	816
SPGR, Z	$P2_1/c$, 2	$Pccn$, 4	$Pccn$, 4	$Pccn$, 4
a, Å	6.4444(5)	25.406(2)	25.296(4)	25.9192(6)
b, Å	5.4336(4)	8.8252(5)	8.8151(9)	8.6303(3)
c, Å	22.795(2)	7.2756(6)	7.327(1)	7.6720(3)
β, deg	89.901(5)	90	90	90
V, Å^3	798.2(1)	1631.3(2)	1633.9(4)	1716.1(1)
R_p, R_{wp}	0.087, 0.125	0.067, 0.093	0.005, 0.007[a]	0.062, 0.084
R_{Bragg}	0.063	0.032	0.006 [a]	0.054

[a] The impressively low values of the figures of merit provided are due to the high number of coefficients used for the description of the background, heavily affected by sample fluorescence.

2.5. Synthesis of Cd(BDMPX) (3). H_2BDMPX (73.5 mg, 0.25 mmol) was dissolved in 15 mL of CH_3OH; $Cd(CH_3COO)_2 \cdot 2H_2O$ (66.6 mg; 0.25 mmol) was then added, and the suspension was stirred at 130 °C in a high-pressure glass tube for 24 h. The white precipitate obtained was filtered off, washed twice with CH_3OH, and then dried under vacuum. Yield: 88%. **3** is insoluble in alcohols, DMSO, acetone, CH_3CN, DMF, and water. IR (cm^{-1}): 3100−3000(vw) ν(C−$H_{aromatic}$), 3000−2800(m) ν(CH_3, CH_2), 1505(vs) ν(C═C+C═N). Elemental analysis calcd for $C_{18}H_{20}CdN_4$ (FW = 404.8 g/mol): C, 53.41; H, 4.98; N, 13.84. Found: C, 53.07; H, 4.96; N, 13.59.

2.6. Synthesis of Cu_2(BDMPX) (4). H_2BDMPX (73.5 mg, 0.25 mmol) was dissolved in 15 mL of CH_3OH; $Cu(CH_3COO)_2$ (45.4 mg; 0.25 mmol) was then added. A green suspension immediately formed which was left under stirring at 130 °C in a high-pressure glass tube for 48 h. The color of the suspension turned progressively from green to white. The white precipitate formed was filtered off, washed twice with methanol, and then dried under vacuum. **4** is insoluble in alcohols, DMSO, acetone, CH_3CN, DMF, and water. IR (cm^{-1}): 3100−3000(vw) ν(C−$H_{aromatic}$), 3000−2800(m and vw) ν(CH_3, CH_2), 1509(vs) ν(C═C+C═N). Elemental analysis calcd for $C_{18}H_{20}Cu_2N_4$ (FW = 419.5 g/mol): C, 51.54; H, 4.81; N, 13.36. Found: C, 51.56; H, 4.47; N, 12.98.

2.7. X-ray Powder Diffraction Structural Analysis. Microcrystalline samples of H_2BDMPX and of compounds **1**−**3** were gently ground in an agate mortar, then they were deposited in the hollow of an aluminum sample holder equipped with a zero-background plate. Diffraction data were collected by means of overnight scans in the 2θ range of 5−105°, with 0.02° steps, on a Bruker AXS D8 Advance diffractometer, equipped with Ni-filtered Cu Kα radiation (λ = 1.5418 Å) and with a Lynxeye linear position-sensitive detector, and mounting the following optics: primary beam Soller slits (2.3°), fixed divergence slit (0.5°), receiving slit (8 mm). The generator was set at 40 kV and 40 mA. A visual inspection of the acquired diffractograms allowed one to purport isomorphism between **1**, **2**, and **3**, which was definitely confirmed by independent indexing. Standard peak search, followed by indexing through the single value decomposition approach[22] implemented in TOPAS-R,[23] allowed the detection of the approximate unit cell parameters of all three species. The space groups were assigned on the basis of the systematic absences. Unit cells and space groups were checked by Le Bail refinements. Structure solutions were performed by the simulated annealing technique, as implemented in TOPAS, employing a semirigid, idealized model for the crystallographic independent portion of the ligand,[24] in which the torsion angles around the methylene groups were allowed to refine. The final refinements were carried out by the Rietveld method, maintaining the semirigid body introduced at the solution stage. The background was modeled by a polynomial function. One refined, isotropic thermal parameter (B_{iso}) was assigned to all the atoms in H_2BDMPX; in **1**−**3**, a refined B_{iso} was attributed to the metal atoms (B_M), lighter atoms being given a $B_{iso} = B_M + 2.0$ Å^2 value. Preferred orientation corrections were introduced (in the March-Dollase formulation) along the [110] direction for species **1**−**3**. Finally, the low-quality data of species **4** prevented any attempt at determining even its unit cell metrics.

Significant crystal data and data collection parameters are gathered in Table 1. Final Rietveld refinement plots are shown in Figure S3 in Supporting Information. Fractional atomic coordinates are supplied in the Supporting Information as CIF files. X-ray crystallographic data in CIF format have been deposited at the Cambridge Crystallographic Data Center as supplementary publications no. 831152−831155. Copies of the data can be obtained free of charge on application to the Director, CCDC, 12 Union Road, Cambridge, CB2 1EZ, UK (Fax: +44−1223−335033; e-mail: deposit@ccdc.cam.ac.uk or http://www.ccdc.cam.ac.uk).

2.8. Thermodiffractometric Studies. Thermodiffractometric experiments were performed on the as-synthesized species **1**−**3** to highlight their "structural" response to temperature increase. The experiments were carried out in air using a custom-made sample heater, assembled by Officina Elettrotecnica di Tenno, Ponte Arche, Italy. Powdered microcrystalline samples of the two species were ground in an agate mortar and deposited in the hollow of an aluminum sample holder. The diffractograms were acquired in a significant low-angle 2θ range, heating in situ, with steps of 20 °C, from 30 °C up to loss of crystallinity. Parametric treatment, with the Le Bail method, of the data acquired before a significant loss of crystallinity allowed us to depict the unit cell parameters variation as a function of the temperature.[25] When comparing the TG and TXRPD results, the reader must be aware that the thermocouple of the TXRPD setup is *not* in direct contact with the sample, this determining a slight difference in the temperature at which the same event is detected by the two techniques. The TG temperatures have to be considered as more reliable.

2.9. Gas Adsorption Measurements. Gas sorption isotherms for pressures in the range of 0−1 bar were measured by the volumetric method using a Beckman Coulter SA 3100 surface area and pore size analyzer instrument. A sample of ca. 50 mg of as-synthesized material was introduced into a preweighed analysis tube (9 mm diameter, 9 cm^3 bulb), capped with a gas-tight transeal to prevent entrance of atmosphere oxygen and of moisture during transfer and weighing. The samples were evacuated under dynamic vacuum (10^{-5} bar) at 150 °C, until a constant weight was achieved. The analysis tube was then weighed again to determine the mass of the evacuated sample. For all isotherms, warm and cold free space correction measurements were performed using ultrahigh purity He gas (UHP grade 5.0, 99.999% purity). N_2 isotherms at 77 K were measured in a liquid nitrogen bath using a UHP-grade gas source.

3. RESULTS AND DISCUSSION

3.1. Synthesis and Crystal Structure of the Ligand H_2B-DMPX. The synthesis of 1,4-bis((3,5-dimethyl-1*H*-pyrazol-4-yl)methyl)benzene (H_2BDMPX) was accomplished improving the two-step approach already proposed in the literature[20] with an optimized procedure to purify the intermediate. Accordingly, by reacting acetylacetone and terephthaldialdehyde, in the

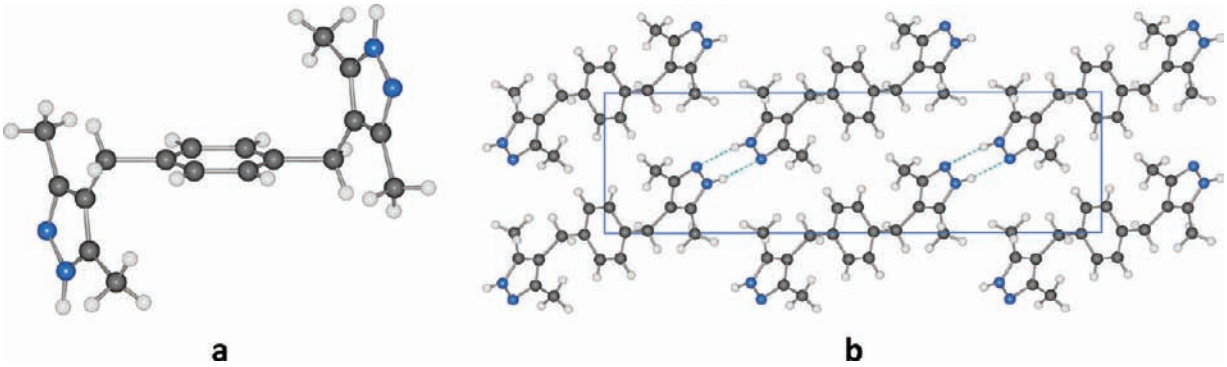

Figure 1. (a) Representation of the molecular structure of H_2BDMPX, highlighting the *anti* conformation adopted by the molecule. (b) Representation, along [010], of the crystal packing in H_2BDMPX, evidencing the network of intermolecular hydrogen bond interactions (cyan dashed lines). Horizontal axis, **c**; vertical axis, **a**. Carbon, gray; hydrogen, white; nitrogen, blue.

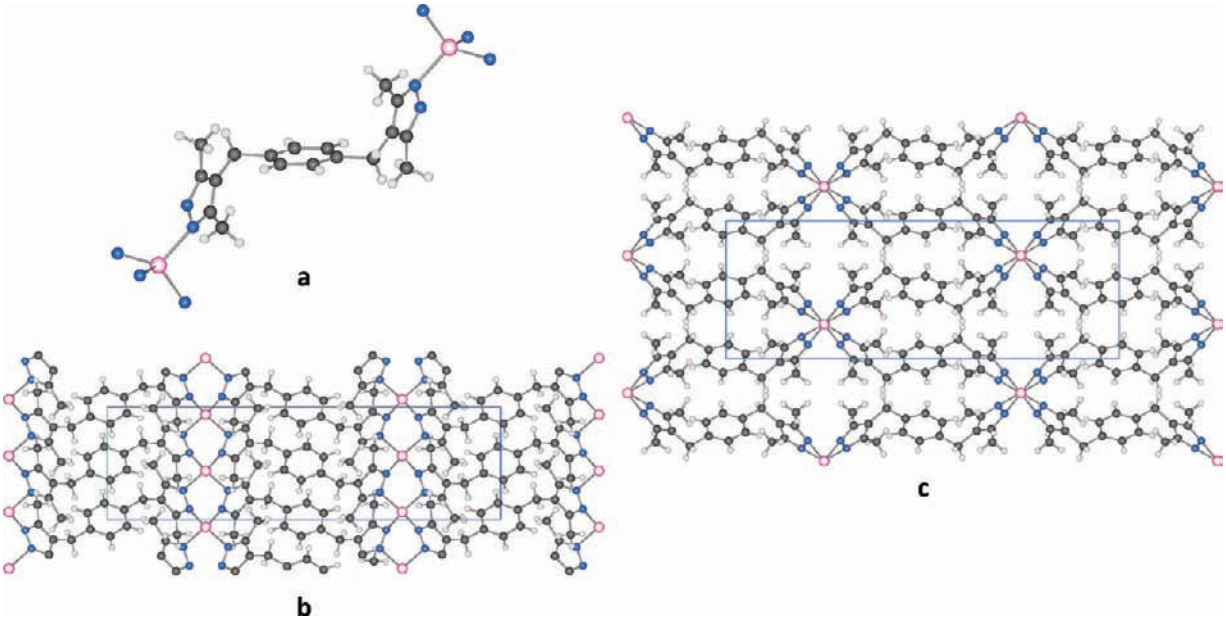

Figure 2. Representation of the crystal structure of **1**: (a) portion of the structure, showing the *anti* conformation adopted by the ligand and the tetrahedral coordination geometry about the Zn(II) ions. (b) Crystal packing viewed along [010], highlighting the 1-D chains of bridged metal ions. Horizontal axis, **a**; vertical axis, **c**. (c) Crystal packing viewed along [001], highlighting the flexible rhombic motifs. Horizontal axis, **a**; vertical axis, **b**. Carbon, gray; hydrogen, white; nitrogen, blue; zinc, purple. The isostructural phases **2** and **3** appear undistinguishable at the drawing level. Significant bond distances (Å) and angles (°): M−N 2.112(7), 2.13(1) (**1**); 2.12(2), 2.18(1) (**2**); 2.23(1), 2.339(5) (**3**); N−M−N 102.8(6), 108.1(5), 112.2(6)° (**1**); 101(1), 109.2(7), 117.4(8) (**2**); 98.4(5), 109.8(6)−121.5(9) (**3**).

presence of trimethylchlorosilane and sodium iodide in acetonitrile, bis(β-diketone)-*p*-xylylene is formed. After purification, the reaction of the latter with an excess of hydrazine hydrate in ethanol at room temperature promotes, by simple condensation, the formation of 1,4-bis((3,5-dimethyl-1*H*-pyrazol-4-yl)methyl)-benzene as a white and air-stable solid.

As can be appreciated in Figure 1, crystals of H_2BDMPX contain individual molecules located onto the crystallographic inversion center of the monoclinic $P2_1/c$ space group. Accordingly, the swinging 4-methylene-3,5-dimethylpyrazole moieties adopt an idealized C_{2h} *anti* conformation, pointing away from the inner aromatic core in opposite directions. This is in accordance with what was observed in the ^{1}H NMR spectrum, where two signals have been found for the not equivalent methyl groups, likely due to the lack of fluxionality, or to a slow interchange of the NH proton between the two heterocyclic nitrogen atoms. As suggested by IR spectroscopy, adjacent individual molecules interact by means of NH···N hydrogen bonds (Figure 1b). Even if rather weak when compared to those characterizing M(pyrazolato) prototypes (N···N 3.2 Å in H_2BDMPX vs 2.9 Å[26]), they nevertheless strengthen the overall crystal structure by defining polyconnected 2-D slabs running normally to the [−1 0 2] direction.

3.2. Synthesis and Crystal Structure of Species 1−4. The solvothermal reaction of Zn(II), Co(II), Cd(II), and Cu(II) acetates with H_2BDMPX in methanol at 130 °C brought the formation of four coordination compounds of formula M_x(BDMPX) (x = 1 for M = Zn, **1**; Co, **2**; Cd, **3**; x = 2 for M = Cu, **4**), isolated as microcrystalline powders in good yield. The same result may be obtained starting from the corresponding

dx.doi.org/10.1021/ic2013705 |*Inorg. Chem.* 2011, 50, 11506–11513

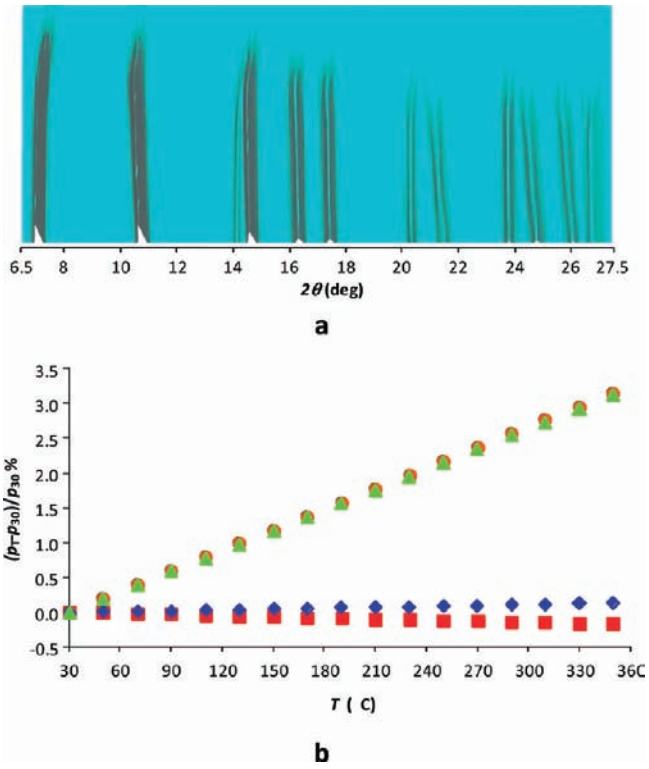

Figure 3. (a) Two-dimensional contour plot of the X-ray powder diffraction patterns measured as a function of the temperature in the range 30−510 °C, highlighting the remarkable thermal stability of species **1**. The flexibility of the framework is appreciable from the non-negligible peak shift. (b) Variation of the unit cell parameters (p_T) of **1** as a function of the temperature, normalized with respect to their value at 30 °C (p_{30}): *a*, red squares; *b*, orange circles; *c*, blue rhombi; *V*, green triangles.

metal(II) nitrates, through 1 day solvothermal reactions carried out in DMF at 130 °C. Incidentally, the high-temperature reaction between copper(II) acetate and H_2BDMPX brings about the reduction of Cu(II) to Cu(I). Indeed, the Cu(II)-containing green suspension observed at the beginning of the reaction is gradually transformed into a Cu(I)-based white precipitate. Reduction of Cu(II)-based pyrazole complexes promoted by heating has already been observed[27] and attributed to the partial oxidation of pyrazole.[28] Thus, the isolation of **4** might be accompanied by the oxidation of either the polyazolate ligand or the methanol employed as solvent.[29]

The isolated coordination compounds are insoluble in most organic solvents, thus suggesting their polymeric nature. As a matter of fact, no N−H stretching can be detected in their IR spectra, indicating the formation of metal-bridging polypyrazolate dianions. More importantly, if practical applications are sought, all of the materials are air-stable and, as verified by TGA and TXRPD, possess remarkably high decomposition temperatures.

The isomorphous compounds **1**−**3** crystallize in the orthorhombic *Pccn* space group. The metal ions, lying on a crystallographic two-fold axis (*c* Wyckoff position) are arranged along 1-D chains running parallel to **c** (Figure 2b), with M···M distances of 3.64 (**1**), 3.66 (**2**), and 3.84 Å (**3**). Along the chains, each M···M vector is bridged by two pyrazolato moieties belonging to two distinct ligands, resulting in a MN_4 tetrahedral

Table 2. Key Parameters Retrieved from the N_2 Adsorption Isotherms of Compounds 1, 2, and 4

	BET specific surface area (m^2/g)	Langmuir specific surface area (m^2/g)	adsorbed N_2 (cm^3/g STP)
1	515(4)	667(2)	153.1
2	209(2)	384(10)	88.1
4	284(5)	420(6)	96.4

coordination geometry at each metal ion. As already observed in the prototypical compounds $M_2(DMPZ)_4(HDMPZ)_2$ (HDMPZ = 3,5-dimethylpyrazole; M = Co,[30] Zn[31]), even in the present case, due to the steric hindrance of the methyl groups in positions 3 and 5 of the heterocyclic rings, the tetrahedral geometry at the metal centers is somewhat distorted, as witnessed by the values of the M−N bond distances and, even more, of the N−M−N angles (see caption to Figure 2). The ligands, located on a crystallographic inversion center (*b* Wyckoff position), adopt the *anti* conformation featured also by H_2BDMPX itself and employ their pyrazolato groups to bridge adjacent 1-D chains, thus defining a 3-D framework (Figure 2c) possessing rhombic motifs. When the local geometrical features of the four structures presented are compared (see Table S1), a substantial constancy of the conformational parameters can be observed, particularly for the three coordination polymers. Due to evident steric hindrance, the pyrazolato ends manifest a rare but already observed twist,[30,31] as evidenced by the values of the M−N−N−M torsion angles, falling near 55° [ideally, a value of 0° is expected, as in M(BDP)[9] and in $Ni_8L_6(OH)_4(H_2O)_2$[15]].

The rhombic motifs envisaged in compounds **1**−**3** recall those present in the flexible metal hydroxyl terephthalates (MIL-53[8d]) and in the M(1,4-BDP) derivatives (M = Ni,[9] Co[10]). In spite of this similarity, as-synthesized **1**−**3** precipitate in a closed-pore form, in which we cannot individuate cavities, channels, or interstices capable to host, *without distortions*, probe molecules. In principle, this feature should not prevent gas adsorption: external stimuli such as temperature, pressure, or probe gas molecules may induce pore-opening/pore-closing processes.[8] Accordingly, when exposed to a probe gas, the title PCPs may adopt an open-pore form, in which the rhombic channels possess a different cross section[32] than in the room conditions closed-form, allowing the probe to enter. This hypothesis was verified by preliminary N_2 adsorption measurements at 77 K, as detailed below.

3.3. Thermal Behavior. The thermal behavior of compounds **1**−**4** was investigated by coupling thermogravimetric analyses (TGA), carried out under N_2, to in situ variable-temperature powder X-ray diffraction experiments (TXRPD), carried out in air. The TG traces are collectively shown in Figure S4; the results of the TXRPD measurements for **1** are reported in Figure 3, while those for **3** are proposed in the Supporting Information as Figure S6.[25]

As expected for a species containing a redox-active metal ion in a partially unstable oxidation state, Cu_2(BDMPX) shows the lowest thermal stability. The latter is nevertheless still significant since the material does not undergo decomposition up to 300 °C. Slightly more stable are the Zn(BDMPX) and Co(BDMPX) species, showing decomposition onsets around 400 °C. Remarkably, Cd(BDMPX) possesses an outstanding robustness, resisting up to about 500 °C.[33] In all cases, a black residue is recovered, likely belonging to carbonaceous species. As anticipated in the

dx.doi.org/10.1021/ic2013705 |*Inorg. Chem.* 2011, 50, 11506–11513

Introduction, the robustness of these materials further confirms the strength of metal−pyrazolato coordination bonds, imparting an unsurpassed stability to the corresponding PCPs.[9,10,13−16]

The above observations are consistent with those retrieved from the TXRPD measurements. The latter confirm the high thermal robustness of species **1**−**3** also in air. More importantly, they show that the frameworks respond to temperature increase with a certain flexibility (Figures 3a and S6a). Parametric Le Bail refinements performed against the acquired data show that the two compounds behave in a way similar to Ni(1,4-BDP).[9] In the case of **1**, while **a** and **c** are basically not affected by the thermal treatment, **b** increases by 3.1%, implying a similar cell volume increment (Figure 3b).

As for **3**, **c** is the less affected axis by the thermal treatment, while **a** and **b** undergo inversely correlated variations, with the two events globally resulting in an inflation of the 3-D framework, with a concomitant unit cell volume maximum increment of 4.2% (Figure S6b). As predictable, flexibility is due to the variation of **a** and **b**, defining the cross section of the rhombic motifs; on the contrary, **c** is the less influenced axis, as expected for the propagation direction of the chains, along which the metal ions are kept at a nearly constant separation by the bridging ligands.

3.4. Gas Adsorption Properties. Prompted by the envisaged framework flexibility, we carried out a preliminary investigation on the permanent porosity of compounds **1**−**3** by collecting N_2 adsorption isotherms at 77 K. For the sake of completeness, the adsorption properties of **4** were studied, as well. Prior to measurements, powdered batches of the compounds were outgassed as detailed in the Experimental Section. As a matter of fact, **1**, **2**, and **4** were found to adsorb significant amounts of N_2 at 77 K (Table 2).

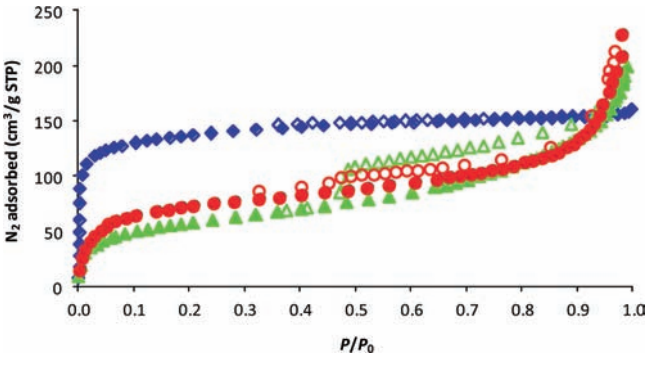

Figure 4. N_2 adsorption isotherms measured at 77 K on **1** (blue rhombi), **2** (green triangles), and **4** (red circles). Filled and empty symbols denote the adsorption and desorption branches, respectively.

On the contrary, the Cd(II) derivative showed no adsorption in the pressure range assayed, even if outgassed at temperatures as high as 250 °C. All of the three adsorbents exhibit a type I adsorption isotherm (Figure 4), with a sharp knee at low relative pressures ($p/p_0 \sim 0.01$), corresponding to the filling of the micropores, followed by a plateau, suggesting that the permanent porosity of the samples is mainly due to micropores of quite uniform size. The presence, in all of the isotherms, of a hysteresis loop is indicative of textural mesoporosity arising from interparticle mesoporous voids.[34]

Fitting the N_2 isotherms, we retrieved BET specific surface areas of 515(4), 209(2), and 284(5) m^2/g, and Langmuir specific surface areas of 667(2), 384(10), and 420(6) m^2/g for **1**, **2**, and **4**, respectively. These results coherently suggest that the closed-pore form observed for **1** and **2** at room temperature is not preserved at 77 K in the presence of N_2, conditions under which the rhombic motifs must possess a different cross section. The absence of adsorption in the case of **3** implies that, despite its isomorphism to **1** and **2** at room conditions, its framework does not undergo the same structural changes purported for **1** and **2** upon adsorption. To explain the persistence of a closed-pore form in **3**, the influence of the stereochemical rigidity of the Cd(II) metal ions, versus the Zn(II) and Co(II) ones, cannot be excluded. As a matter of fact, as reported in the extensive stereochemical analysis carried out by Cirera and co-workers,[35] the stereochemical flexibility of the ZnN_4 chromophores is higher than that of the Cd(II) analogues.

The behavior of **1** and **2** is not surprising: as already evidenced in the case of $[Cu(Hoxonato)(bpy)_{0.5}]n\cdot 1.5nH_2O$ (H_3oxonic: 4,6-dihydroxy-1,3,5-triazine-2-carboxylic acid),[36] a *porosity without pores* phenomenon may successfully occur when a rearrangement (or sliding) of the structural motifs is induced by suitable external stimuli, obviously maintaining the complete connectivity without bond breaking. Thus, **1** and **2** are to be considered as notable representatives of the class of *pro-porous* materials, in which flexibility, prompted by an ad hoc external stimulus, brings about permanent porosity.

3.5. Photoluminescence Properties. Preliminary tests carried out in the solid state on species **1**, **3**, and **4** revealed that they give distinct responses when exposed to UV irradiation at

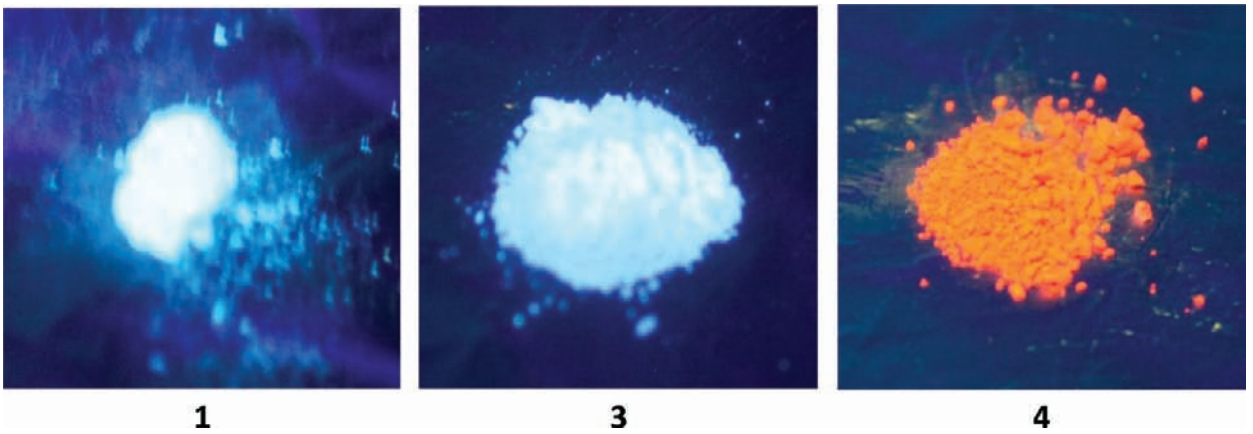

Figure 5. Visible effect of the photoluminescence manifested by **1**, **3**, and **4** after UV irradiation.

dx.doi.org/10.1021/ic2013705 |*Inorg. Chem.* 2011, 50, 11506–11513

room temperature (Figure 5): **1** and **3** give a near-white photoluminescence emission when excited at 365 nm; an orange emission is at variance observed when **4** is irradiated at 254 nm. When irradiated at 365 nm, the Zn(II) derivative **1** gives a single, broad emission band in the near-UV region, its maximum lying at 380 nm. When excited at 254 nm, the Cd(II) homologous **3** gives two broad and partially superimposed emission bands with maxima at 353 and 378 nm. Finally, when excited at 400 nm, the Cu(I) species **4** gives one broad band in the visible region, with maximum at 597 nm. The high-energy emissions shown by **1** and **3** may be confidently attributed to ligand-based [$\pi-\pi^*$] excited states,[37] with no involvement of the metal centers. On the contrary, the low-energy photoluminescence emission of **4** is reasonably due to a metal-to-ligand charge transfer (MLCT) excited state, as is typical for Cu(I) complexes, in which the ligand LUMO orbitals are sufficiently low in energy to accept an excited electron from the electron-rich metal center.[38]

4. CONCLUSIONS

The four coordination compounds M_x(BDMPX) (x = 1 for M = Zn, **1**; Co, **2**; Cd, **3**; x = 2 for M = Cu, **4**) were prepared by solvothermal reactions involving the flexible, pyrazole-based, 1,4-bis((3,5-dimethyl-1*H*-pyrazol-4-yl)methyl)benzene ligand (H_2BDMPX) and were fully characterized. All of them possess a high thermal robustness, as witnessed by their stability in air at least up to 300 °C. The species **1**−**3** feature a closed-pore 3-D network, in which rhombic motifs can be recognized. Interestingly, a certain framework flexibility toward an open-pore form is brought about, in the case of **1** and **2**, by N_2 adsorption at 77 K. Thus, **1** and **2** are a notable example of pro-porous materials, their adsorption performances implying a low-temperature opening of the rhombic motifs, stimulated by the gas probe and facilitated by the nature of the ligand.

■ ASSOCIATED CONTENT

Supporting Information. Details on the synthesis of H_2BDMPX. IR spectroscopy for H_2BDMPX and for species **1**−**4**, ^{1}H NMR for H_2BDMPX. Rietveld refinement plots for H_2BDMPX, **1**, and **3**. TXRPD traces for **2** and **3**. TXRPD data treatment for **3**. Comparative structural analysis of molecular conformations in H_2BDMPX and in **1**−**3**. Crystallographic data for species **1**−**3** in CIF format. This material is available free of charge via the Internet at http://pubs.acs.org.

■ AUTHOR INFORMATION

Corresponding Author

*E-mail: aurel.tabacaru@unicam.it (A.T.), simona.galli@uninsubria.it (S.G.).

■ ACKNOWLEDGMENT

Special thanks are addressed to Dr. Ivan Timokhin and Dr. Stefano Lancianesi for sharing useful ideas, as well as to University of Camerino (UNICAM) for funding.

■ REFERENCES

(1) (a) MacGillivray, L. R., Ed. *Metal−Organic Frameworks: Design and Application*; John Wiley & Sons Inc: Hoboken, NJ, 2010. (b) Schöder, M., Ed. *Functional Metal−Organic Frameworks: Gas Storage, Separation and Catalysis*; Springer: Berlin, 2010. (c) Meek, S. T.; Greathouse, G. A.; Allendorf, M. D. *Adv. Mater.* **2010**, *23*, 249–267.

(2) (a) Park, K. S.; Ni, Z.; Côté, A. P.; Choi, J. Y.; Huang, R.; Uribe-Romo, F. J.; Chae, H. K.; O'Keeffe, M.; Yaghi, O. M. *Proc. Natl. Acad. Sci. U.S.A.* **2006**, *103*, 10186–10191. (b) Mathivathani Kandiah, M.; Nilsen, M. H.; Usseglio, S.; Jakobsen, S.; Olsbye, U.; Tilset, M.; Larabi, C.; Quadrelli, E. A.; Bonino, F.; Lillerud, K. P. *Chem. Mater.* **2010**, *22*, 6632–6640.

(3) (a) Wang, Z.; Cohen, S. M. *Chem. Soc. Rev.* **2009**, *38*, 1315–1329. (b) Tanabe, K. K.; Cohen, S. M. *Chem. Soc. Rev.* **2011**, *40*, 498–519.

(4) (a) Férey, G.; Serre, C.; Devic, T.; Maurin, G.; Jobic, H.; Llewellyn, P. L.; De Weireld, G.; Vimont, A.; Daturi, M.; Chang, J.-S. *Chem. Soc. Rev.* **2011**, *40*, 550–562. (b) Ma, S.; Zhou, H.-C. *Chem. Commun.* **2010**, *46*, 44–53. (c) Murray, L. J.; Dinca, M.; Long, J. R. *Chem. Soc. Rev.* **2009**, *38*, 1294–1314. (d) Morris, R. E.; Wheatley, P. S. *Angew. Chem., Int. Ed.* **2008**, *47*, 4966–4981.

(5) (a) Czaja, A. U.; Trukhan, N.; Muller, U. *Chem. Soc. Rev.* **2009**, *38*, 1284–1293. (b) Li, J. R.; Kuppler, R. J.; Zhou, H. C. *Chem. Soc. Rev.* **2009**, *38*, 1477–1504. (c) Liu, D.; Zhong, C. *J. Mater. Chem.* **2010**, *20*, 10308–10318.

(6) (a) Ma, L. Q.; Abney, C.; Lin, W. B. *Chem. Soc. Rev.* **2009**, *38*, 1248–1256. (b) Lee, J.-Y.; Farha, O. K.; Roberts, J.; Scheidt, K. A.; Nguyen, S. T.; Hupp, J. T. *Chem. Soc. Rev.* **2009**, *38*, 1450–1459. (c) Farrusseng, D.; Aguado, S.; Pinel, C. *Angew. Chem., Int. Ed.* **2009**, *48*, 7502–7513.

(7) (a) Horcajada, P.; Chalati, T.; Serre, C.; Gillet, B.; Sebrie, C.; Baati, T.; Eubank, J. F.; Heurtaux, D.; Clayette, P.; Kreuz, C.; Chang, J.-S.; Hwang, Y. K.; Marsaud, V.; Bories, P.-N.; Cynober, L.; Gil, S.; Férey, G.; Couvreur, P.; Gref, R. *Nat. Mater.* **2010**, *9*, 172. (b) Imaz, I.; Rubio-Martínez, M.; García-Fernández, L.; García, F.; Ruiz-Molina, D.; Hernando, J.; Puntes, V.; Maspoch, D. *Chem. Commun.* **2010**, *46*, 4737. (c) Ke, F.; Yuan, Y.-P.; Qiu, L.-G.; Shen, Y.-H.; Xie, A.-J.; Zhu, J.-F.; Tian, X.-Y.; Zhang, L. D. *J. Mater. Chem.* **2011**, *21*, 3843–3848.

(8) (a) Kitagawa, S.; Kondo, M. *Bull. Chem. Soc. Jpn.* **1998**, *71*, 1739–1753. (b) Kazuhiro Uemura, K.; Matsuda, R.; Kitagawa, S. *J. Solid State Chem.* **2005**, *178*, 2420–2429. (c) Bradshaw, D.; Claridge, J. B.; Cussen, E. J.; Prior, T. J.; Rosseinsky, M. J. *Acc. Chem. Res.* **2005**, *38*, 273–282. (d) Férey, G.; Serre, C. *Chem. Soc. Rev.* **2009**, *38*, 1380–1399.

(9) Galli, S.; Masciocchi, N.; Colombo, V.; Maspero, A.; Palmisano, G.; López-Garzón, F. J.; Domingo-García, M.; Fernández-Morales, I.; Barea, E.; Navarro, J. A. R. *Chem. Mater.* **2010**, *22*, 1664–1672.

(10) (a) Choi, H. J.; Dincă, M.; Long, J. R. *J. Am. Chem. Soc.* **2008**, *130*, 7848–7850. (b) Salles, F.; Maurin, G.; Serre, C.; Llewellyn, P. L.; Knöfel, C.; Choi, H. J.; Filinchuk, Y.; Oliviero, L.; Vimont, A.; Long, J. R.; Férey, G. *J. Am. Chem. Soc.* **2010**, *132*, 13782–13788.

(11) (a) Masciocchi, N.; Galli, S.; Sironi, A. In *Techniques in Inorganic Chemistry*; Fackler, J. P., Falvello, L., Eds.; CRC Press Taylor and Francis: Boca Raton, FL, 2010. (b) Huang, X.-C.; Lin, Y.-Y.; Zhang, J.-P.; Chen, X.-M. *Angew. Chem., Int. Ed.* **2006**, *45*, 1557–1559. (c) Tian, Y.-Q.; Zhao, Y.-M.; Chen, Z.-X.; Zhang, G.-N.; Weng, L.-H.; Zhao, D.-Y. *Chem.—Eur. J.* **2007**, *13*, 4146–4154. (d) Demessence, A.; D'Alessandro, D. M.; Foo, M. L.; Long, J. R. *J. Am. Chem. Soc.* **2009**, *131*, 8784–8786.

(12) (a) Greathouse, J. A.; Allendorf, M. D. *J. Am. Chem. Soc.* **2006**, *128*, 10678–10679. (b) Kaye, S. S.; Dailly, A.; Yaghi, O. M.; Long, J. R. *J. Am. Chem. Soc.* **2007**, *129*, 14176–14177. (c) Low, J. J.; Benin, A. I.; Jakubczak, P.; Abrahamian, J. F.; Faheem, S. A.; Willis, R. R. *J. Am. Chem. Soc.* **2009**, *131*, 15834–15842.

(13) Zhang, J.-P.; Kitagawa, S. *J. Am. Chem. Soc.* **2008**, *130*, 907–917.

(14) Choi, H. J.; Dincă, M.; Dailly, A.; Long, J. R. *Energy Environ. Sci.* **2010**, *3*, 117–123.

(15) Masciocchi, N.; Galli, S.; Colombo, V.; Maspero, A.; Palmisano, G.; Seyyedi, B.; Lamberti, C.; Bordiga, S. *J. Am. Chem. Soc.* **2010**, *132*, 7902–7904.

(16) Colombo, V.; Galli, S.; Choi, H. J.; Han, G. D.; Maspero, A.; Palmisano, G.; Masciocchi, N.; Long, J. R. *Chem. Sci.* **2011**, *2*, 1311–1319.

(17) Férey, G. *Chem. Soc. Rev.* **2008**, *37*, 191–214.

(18) Kitaura, R.; Fujimoto, K.; Noro, S.-I.; Kondo, M.; Kitagawa, S. *Angew. Chem., Int. Ed.* **2002**, *41*, 133–135.

(19) Korshak, V. V.; Krongaus, E. S.; Berlin, A. M. *J. Polym. Sci., Part A* **1965**, *3*, 2425–2439.
(20) Muehlebach, A. Ciba Geigy AG, European Patent 532461A1.
(21) Trofimenko, S. *J. Am. Chem. Soc.* **1970**, *92:17*, 5118–5126.
(22) Coelho, A. *J. Appl. Crystallogr.* **2003**, *36*, 86–95.
(23) *TOPAS*, version 3.0; Bruker AXS, Karlsruhe, Germany, 2005.
(24) To describe the ligand, the *z*-matrix formalism was used, imposing idealized bond distances and angles, as follows: C−C, C−N, N−N of the heterocyclic ring 1.36 Å; C−C of the arene 1.39 Å; exocyclic C−C 1.50 Å; C−H, N−H = 0.95 Å; heterocyclic ring internal bond angles 108°; arene internal and external bond angles 120°.
(25) In the case of **2**, due to the Co-K fluorescence affecting its diffractograms, the TXRPD measurements are commented only on a qualitative basis, the parametric Le Bail treatment of the data being somehow hampered. Its TXRPD traces have been included in the Supporting Information (Figure S5).
(26) Masciocchi, N.; Moret, M.; Cairati, P.; Sironi, A.; Ardizzoia, G. A.; La Monica, G. *J. Am. Chem. Soc.* **1994**, *116*, 7668–7676.
(27) Ehlert, M. K.; Rettig, S. J.; Storr, A.; Thompson, R. C.; Trotter, J. *Can. J. Chem.* **1990**, *68*, 1444–1449.
(28) Schofield, K.; Grimmet, M. R.; Keene, B. R. T. *Heteroaromatic Nitrogen Compounds: The Azoles*; Cambridge University Press: Cambridge, 1976; p 154.
(29) Attempts to carry out the synthesis of a Cu(II) derivative working at room temperature in different solvents resulted in green, possibly Cu(II)-based, precipitates, whose preliminary characterization revealed that they are mixtures of phases difficult to be purified.
(30) Ehlert, M. K.; Rettig, S. J.; Storr, A.; Thompson, R. C.; Trotter, J. *Can. J. Chem.* **1993**, *71*, 1425–1436.
(31) Ehlert, M. K.; Rettig, S. J.; Storr, A.; Thompson, R. C.; Trotter, J. *Can. J. Chem.* **1990**, *68*, 1494–1498.
(32) Millange, F.; Serre, C.; Guillou, N.; Férey, G.; Walton, R. *Angew. Chem., Int. Ed.* **2008**, *47*, 4100–4105.
(33) The small drift at low temperature is possibly related to moisture or to a negligible percentage of organic contaminant.
(34) Rouquerol, F.; Rouquerol, J.; Singh, K. S. S. *Adsorption by Powders and Porous Solids*; Academic Press: New York, 1999.
(35) Cirera, J.; Alemany, P.; Alvarez, S. *Chem.—Eur. J.* **2004**, *10*, 190–207.
(36) Barea, E.; Tagliabue, G.; Wang, W. G.; Pérez-Mendoza, M. J.; Mendez-Liñan, L.; López-Garzon, F. J.; Galli, S.; Masciocchi, N.; Navarro, J. A. R. *Chem.—Eur. J.* **2010**, *16*, 931–937.
(37) Zhang, J.-P.; Chen, X.-M. *Chem. Commun.* **2006**, 1689–1699.
(38) Zhang, J.-P.; Lin, Y. Y.; Huang, X. C.; Chen, X. M. *J. Am. Chem. Soc.* **2005**, *127*, 5495–5506.